Neuro-Oncology 14(12):1465–1472, 2012.
doi:10.1093/neuonc/nos258
Advance Access publication October 22, 2012

Detection of 2-hydroxyglutaric acid in vivo by proton magnetic resonance spectroscopy in U87 glioma cells overexpressing isocitrate dehydrogenase–1 mutation

Jelena Lazovic, Horacio Soto, David Piccioni, Jerry R. Lo Ru, Sichen Li, Leili Mirsadraei, William Yong, Robert Prins, Linda M. Liau, Benjamin M. Ellingson, Timothy F. Cloughesy, Albert Lai, and Whitney B. Pope

Department of Radiological Sciences (J.L., B.M.E., W.B.P.); Department of Neurosurgery (H.S., J.R.L.R., R.P., L.M.L.); Department of Neurology (D.P., S.L., T.F.C., A.L.); Department of Pathology and Laboratory Medicine, David Geffen School of Medicine, University of California, Los Angeles, California (L.M., W.Y.)

The arginine 132 (R132) mutation of isocitrate dehydrogenase –1 (*IDH1*^{R132}) results in production of 2-hydroxyglutarate (2-HG) and is associated with a better prognosis compared with wild-type (WT) in glioma patients. The majority of lower-grade gliomas express IDH1^{R132}, whereas this mutation is rare in grade IV gliomas. The aim of this study was to noninvasively investigate metabolic and physiologic changes associated with the *IDH1* mutation in a mouse glioma model. Using a 7T magnet, we compared MRI and proton magnetic resonance spectroscopy (MRS) in U87 glioma cells overexpressing either the mutated *IDH1*^{R132} or *IDH1* wild-type (*IDH1*^{WT}) gene in a mouse flank xenograft model. Flank tumors overexpressing IDH1^{R132} showed a resonance at 2.25 ppm corresponding to the 2-HG peak described for human IDH1^{R132} gliomas. WT tumors lacked this peak in all cases. IDH1 mutant tumors demonstrated significantly reduced glutamate by in vivo MRS. There were no significant differences in T_2, apparent diffusion coefficient (ADC), or perfusion values between the mutant and IDH1^{WT} tumors. The IDH1^{R132} mutation results in 2-HG resonance at 2.25 ppm and a reduction of glutamate levels as determined by MRS. Our results establish a model system where 2-HG can be monitored noninvasively, which should be helpful in validating 2-HG levels as a prognostic and/or predictive biomarker in glioma.

Received February 27, 2012; accepted August 23, 2012.

Corresponding Author: Whitney B. Pope, MD, PhD, Department of Radiological Sciences, UCLA Radiology Sciences, 757 Westwood Blvd., Ronald Reagan UCLA Medical Center, room #1621, Los Angeles, CA 90095 (wpope@mednet.ucla.edu).

Keywords: animal models, glioblastoma, glioma, isocitrate dehydrogenase 1 (IDH1), MRI, MRS.

A comprehensive genomic analysis of human glioblastoma multiforme (GBM) in 2008 revealed a mutation in the active site of isocitrate dehydrogenase–1 (*IDH1*) (without loss of heterozygosity) in 12% of GBM patients.[1] Over the past 3 years, additional studies have reported the presence of the *IDH1* mutation in acute myeloid leukemia,[2–4] acute lymphoblastic leukemia,[5] prostate cancer,[5] colorectal cancer,[6] and melanoma.[7] Subsequent investigation confirmed the presence of a point mutation affecting arginine at residue 132 (R132) of the IDH1 protein (IDH1^{R132}) in >70% of lower-grade gliomas.[8] The R132 residue is conserved among species, likely representing the substrate binding site.[9] *IDH1*^{R132} appears to be an early event in gliomagenesis before the emergence of the p53 mutation,[10] leading to the speculation that it contributes to malignant transformation. Median overall survival among patients with anaplastic astrocytoma harboring mutations in either the *IDH1* or *IDH2* gene is significantly longer than that among patients without these mutations (65 vs 20 months).[8] Similarly, glioblastoma patients with mutated *IDH1* or *IDH2* have a median survival of 31 months v 15 months for patients with *IDH* wild-type (*IDH*^{WT}).[1,8]

In 2009, Dang et al.[11] reported that IDH1^{R132} in gliomas is associated with the production of 2-hydroxyglutarate (2-HG), instead of α-ketoglutarate, and proposed a potential "gain of function" effect, rather than just a dominant inhibition of IDH1 catalytic activity. The same study also determined that the carbon source for 2-HG production is derived from glutamine

after oxidation to α-ketoglutarate. Reduced levels of α-ketoglutarate were reported as a consequence of $IDH1^{R132}$,[12] suggesting that this mutation may also influence metabolism. Whether oncogenic potential can derive from 2-HG, as previously speculated,[11,13,14] or from metabolic changes related to $IDH1^{R132}$ is still under investigation.

Based on these data, 2-HG has been proposed as a potential biomarker for patients with glioma. Investigating this possibility, multiple researchers,[15–17] including our own group,[18] have used proton magnetic resonance spectroscopy (MRS) to noninvasively measure 2-HG levels in human glioma patients. However, gliomas are heterogeneous tumors both genetically and metabolically,[19] so it is difficult to control for tumor differences not related to the IDH1 mutation in human patients (eg, tumor grade or other oncogenic mutations). Conversely, the U87 mouse glioma model presents an opportunity to compare IDH1 mutant and WT tumors in a controlled environment.

Thus, in this study, we used human U87 glioma cells transfected with $IDH1^{R132}$ in order to study the consequences of $IDH1^{R132}$ overexpression on tumor imaging features, physiology, and metabolism. This is the first step in establishing a well-characterized experimental model system in order to test the ability of noninvasive 2-HG measures to act as a biomarker of glioma growth and treatment response.

Methods

Cell Lines and the Generation of Constructs

All cells were cultured at 37°C and 5% CO_2 in a 90% humidified tissue incubator. Culture medium was composed of Dulbecco's modified Eagle's medium/F12 medium supplemented with 10% fetal bovine serum (FBS), 2 mM glutamine, and 100 units/mL of penicillin/streptomycin. Human WT *IDH1* coding sequences were amplified from U87 malignant glioma (MG) cells. The cDNA was fused in-frame with a FLAG tag at the C-terminus by the adapter primers (forward primer with the XhoI site underlined: 5′-TACTCGAGATGTCCAAAAAAATCAGTGG-3′, reverse primer with the EcoRI site underlined and the FLAG tag italicized: 5′-ACGAATTC*TTACTTGTCATCGTCATCCTTGTAATCCAT*AAGTTTGGCCTG-3′) and inserted into a XhoI- and EcoRI-linearized pLPCX vector. The $IDH1^{R132H}$ alteration was generated in pLPCX-IDH1-WT-FLAG using the Quikchange method (Stratagene) with the following primer sequence: 5′R132H (5′-ACCTATCATCATAGGTCATCATGCTTATGGG-3′) and 3′R132H (5′-TGACCTATGATGATAGGTTTTACCCATCCAC-3′). A FuGene HD transfection system (Roche) was used to transfect plat-A cells with pLPCX-IDH1-ΔR132H-Flag, pLPCX-IDH1-WT-Flag, and vector control pLPCX-Flag constructs. U87 cells were infected with a retrovirus produced by plat-A package cells in medium containing 8 μg/mL polybrene. After 48 h, cells were selected with 0.7 μg/mL puromycin. Protein expression was confirmed by immunoblot and immunofluorescence (data not shown).

Animal Model

All animal experiments were approved by the University of California at Los Angeles Institutional Animal Care and Use Committee. Male NOD-*scid* mice (6–8 weeks old) were used for all experiments except 2-HG injection, where a phosphatase and tensin homolog (PTEN)/K-Ras knockout mouse was used (see below). Three groups of NOD-*scid* mice were injected with 10^6 glioma cells into the right flank as follows: (i) $IDH1^{WT}$-U87 cells ($n = 7$); (ii) mock-transfected U87 cells (U87-vector control) ($n = 2$); and (iii) U87 cells transfected with the $IDH1^{R132}$ construct ($n = 8$).

Magnetic Resonance Imaging and ^{1}H Magnetic Resonance Spectroscopy

MRI and MRS were performed on a 7T Bruker system with a custom-built 2.2-cm radiofrequency birdcage coil. Mice were imaged at 14 and 21 days following glioma cell injections. Before imaging, we anesthetized the animals with isoflurane (4% induction, maintenance with 1.5%). During imaging, respiration was monitored and isoflurane levels were adjusted if breathing was <20 or >60 breaths per minute. Mice were kept warm with water heated to 37°C circulated using a TP500 water pump (Gaymar Solid State). To quantify T_2 of different tumors, a multislice multi-echo (MSME) spin echo sequence was used (repetition time (TR)/echo time (TE) = 2000/7.26–101.64 ms, 14 echoes, 78 μm^2 in-plane resolution, 1-mm slice thickness, number of experiments [NEX] = 2). A diffusion-weighted imaging–echo planar imaging (DWI-EPI) sequence (TR/TE = 3800/22.03 ms, with 3 *b*-values: 0, 500, 1000; 3 diffusion directions; and 156^2 μm^2 resolution; 1-mm slice thickness; NEX = 2) was used to measure ADC. Nonlinear least-squares regression was used to estimate ADC from multiple *b*-value DWIs and T_2 from MSME data on a voxel-wise basis. Dynamic susceptibility contrast (DSC) perfusion MRI was collected using an EPI readout with 500 ms temporal resolution (2 slices; TR/TE = 500/7.18 ms; flip-angle = 45 degrees; 312^2 μm^2 in-plane resolution; 0.5-mm slice thickness; NEX = 1; 360 repetitions) following tail-vein injection of 0.05 mL of 0.5 mol/L gadolinium-based contrast agent (Magnevist, Berlex). Following DSC-MRI, we acquired a postcontrast T1-weighted spin-echo dataset (1-mm thick slices, TR/TE 500/7.3 ms, 78 μm^2 resolution, 2 NaX).

Perfusion data were processed offline using ImageJ (National Institutes of Health; rsbweb.nih.gov/ij/), and the DSCoMAN plugin was written by Daniel Barboriak (Duke University, https://dblab.duhs.duke.edu/wysiwyg/downloads/DSCoMAN_1.0.pdf). DSC-MRI analysis consisted of truncating the first 5 time points in the DSC-MRI time series to ensure

steady-state magnetization, calculating the pre-bolus signal intensity on a voxel-wise basis, converting the truncated DSC-MRI time series to a concentration-time curve based on the T_2^* relaxivity of the contrast agent, and estimating relative tumor blood flow (rTBF) on a voxel-wise basis by using the first moment of the delta R2 (R2 = 1/T2) curves to calculate mean transit time and with leakage correction to calculate tumor blood volume as described in a previous publication.[20]

MRS was performed using a point-resolved spectroscopic sequence (TR/TE = 4000/6.9 ms; NEX = 512; 3-mL voxel volume within the tumor) and a variable pulse power and optimized relaxation delay water suppression scheme.[21] MRS data were quantified using the LCModel,[22] and 2-HG was modeled based on J-coupling.[23] To optimize detection of 2-HG, MRS was performed on a 2-HG phantom (1-M concentration) using multiple TE times (6.9–30 ms, with 5-ms increments). We found the strongest signal-to-noise ratio for the 2-HG peak in the spectra with the shortest TE (~6.9 ms). Importantly, glutamate resonance (at 2.31–2.35 ppm) was distinct from 2-HG resonance (at 2.24–2.26 ppm). Metabolites with standard deviation (Cramer–Rao lower bounds) less than 20% of the estimated metabolite concentration were considered. Relative metabolite concentrations were expressed with respect to choline, since creatine levels were very low. This choice was justified by the lack of significant difference in the absolute choline concentration observed among the flank tumors.

Validation of 2-HG Chemical Shift on MRS in a PTEN/K-Ras Knockout Mouse

Validation of the precise 2-HG chemical shift on the MRS spectrum was determined by injecting exogenous 2-HG (Santa Cruz Biotechnology) into a PTEN/K-Ras knockout mouse[24] with a 3-mm optic glioma. This model was chosen to ensure maximum delivery of 2-HG to the tumor, since flank tumors have relatively poor perfusion and areas with limited contrast-agent uptake. Phosphate buffered saline (PBS) was used to prepare 1 M 2-HG solution, and pH was adjusted to 7.4. Serum concentration following a 0.1-mL injection of 1 M 2-HG for a 15-g mouse was ~10 mM. MRS was performed before and 30 min after 2-HG injection with a similar protocol as previously described, with the exception of NEX = 256 and a 2.5-mL voxel volume, which covered the tumor.

Histology and Immunohistochemistry

Following noninvasive MRI and MRS examinations, mice were anesthetized with pentobarbital (100 mg/kg i.p.) and sacrificed. The tumor tissue was fixed by immersion into 4% formalin overnight and then embedded in paraffin. Sections (10-μm thick) were cut, deparaffinized, and stained by standard hematoxylin and eosin (H&E) technique. Tumor necrosis was scored using H&E stained slides. Degree of necrosis was estimated from ≥2 adjacent sections by 2 experienced neuropathologists (W.Y. and L.M.). The percent of necrosis was calculated as necrotic area within the tumor v the whole area of the tumor and expressed as a fraction of 100 to the nearest decile. In addition, adjacent slices were processed with mouse anti-human antibody specific for $IDH1^{R132H}$ mutation[25] (Dianova) for immunohistochemistry. Sections were processed using the Dako EnVision+ system (peroxidase) with blocking steps and secondary antibody dilutions per the manufacturer's instructions (DakoCytomation). NovaRED (Vector Laboratories) was used as a chromogen. Mayer's hematoxylin was used as a counterstain.

Statistical Analysis

MRS metabolites, T_2, and ADC values within different tumor volumes were analyzed using an analysis of variance (ANOVA) across groups (U87-$IDH1^{R132}$, U87-$IDH1^{WT}$, U87-vector). The Holm–Sidak test for multiple pairwise comparisons was used for post hoc comparisons. Sigma Stat 11.0 (Systat Software) was used for ANOVA analysis. $P < .05$ was considered statistically significant. Data are given as means ± standard deviation (SD) unless stated otherwise.

Results

Validation of 2-HG Chemical Shift Assignment in MRS Spectra

Validation of the chemical shift assigned to 2-HG on the ^{1}H-MR spectrum was performed using 0.1 mL of 1 M 2-HG solution injected into a PTEN/K-Ras mouse with an optic glioma. After 30 min following 2-HG injection, a distinct peak appeared at ~2.25 ppm, the expected location based on J-coupling simulations using the LCModel (Fig. 1B). This chemical shift corresponded to the strongest peak of 2-HG (hydrogen attached to C-4 of 2-HG), similar to previously published results for 2-HG using J-coupling modeling and MRS.[23]

Measurement of 2-HG in Tumors Overexpressing $IDH1^{R132}$

Quantitative MRS using the LCModel algorithm with J-coupling modeling for 2-HG confirmed the presence of a 2-HG peak in all U87 flank tumors overexpressing $IDH1^{R132}$, whereas 2-HG levels were not detectable in $IDH1^{WT}$ U87 and U87-vector tumors (Fig. 2). The presence of 2-HG in $IDH1^{R132}$ flank tumors was associated with a significant decrease of glutamate ($P < .05$, ANOVA with Holm–Sidak post hoc test) (Fig. 2C and D) compared with $IDH1^{WT}$ and vector control tumors. The ratios of lactate:choline and glutathione:choline (thought to be a measure of oxidative stress) were not significantly different between $IDH1^{R132}$ and $IDH1^{WT}$ tumors (Fig. 2D). The lactate levels, however, in the vector control tumors were significantly reduced

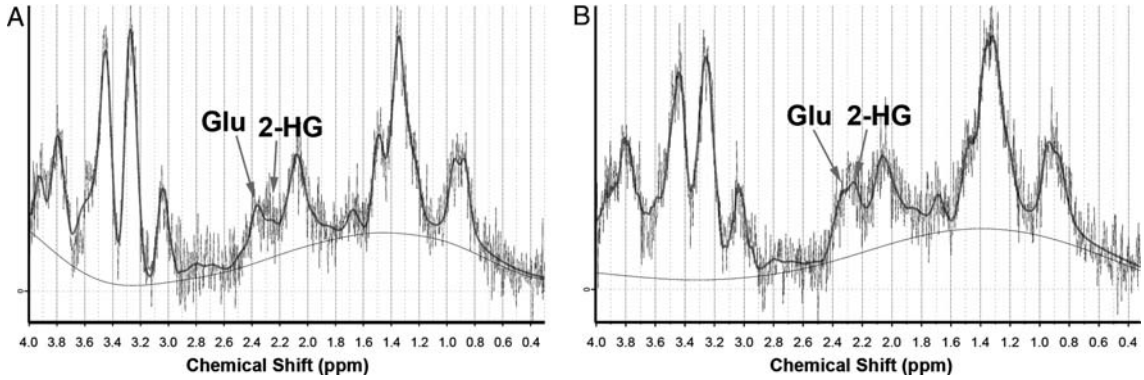

Fig. 1. Verification of 2-HG detection and chemical shift. A PTEN/K-Ras knockout mouse with optic glioma was injected with 0.1 mL of 1 M 2-HG and subjected to MRS before and 30 min after injection. (A) MRS spectrum before injection showing baseline metabolites of the optic glioma. (B) After 30 min following i.v. injection, we noticed the emergence of the additional peak at ~2.25 ppm that we assigned to 2-HG.

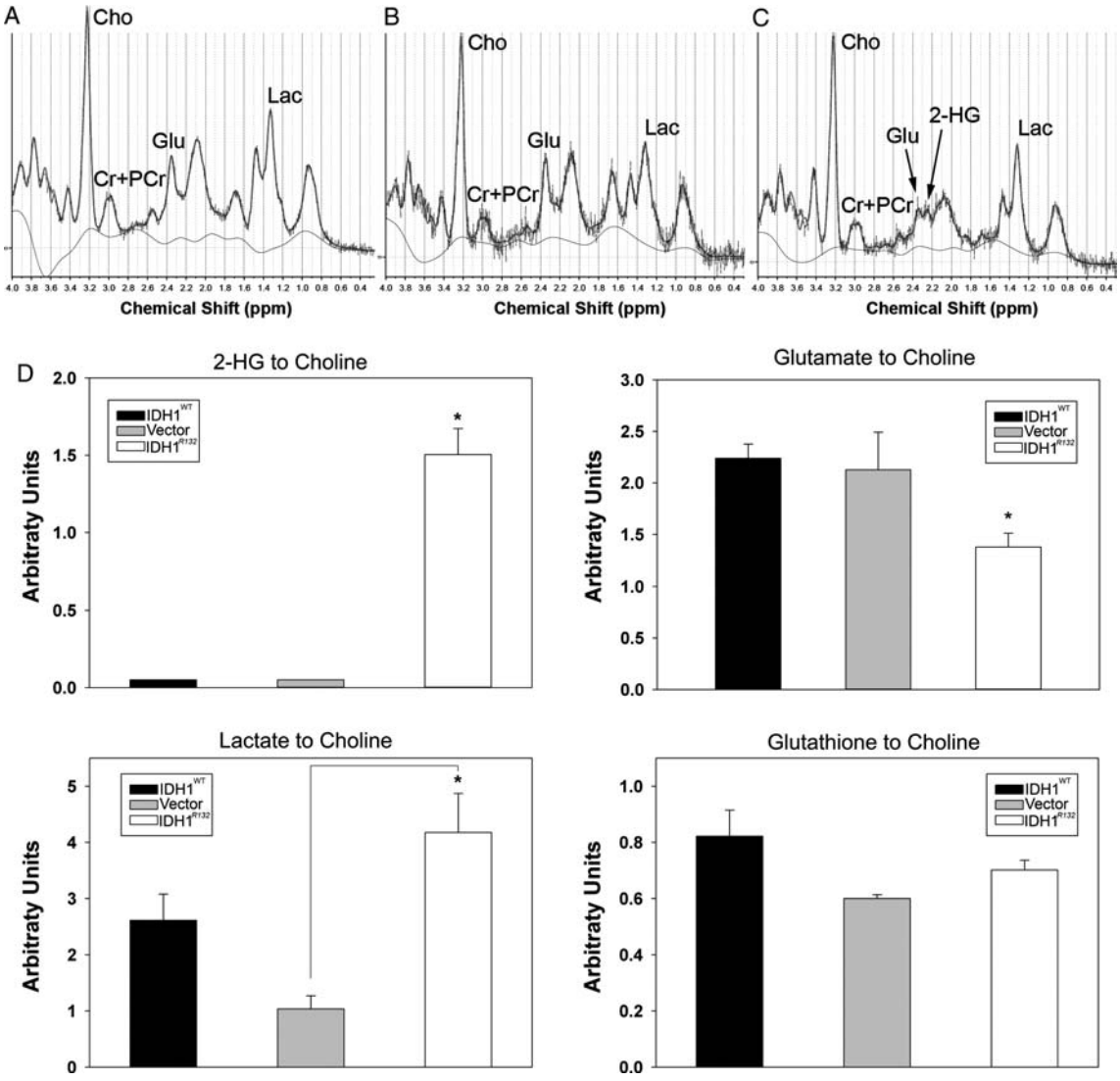

Fig. 2. Representative 1D MRS spectrum of (A) IDH1^{WT}, (B) vector-control, and (C) tumors overexpressing IDH1^{R132}. Notice the reduced glutamate/glutamine peak and additional peak corresponding to 2-HG at ~2.25 ppm in IDH1^{R132} flank tumors. (D) Concentration of 2-HG, glutamate, lactate, and glutathione as a ratio to choline (arbitrary units) expressed as mean ± SD. *$P < .05$ ANOVA with Holm–Sidak correction for multiple pairwise comparison.

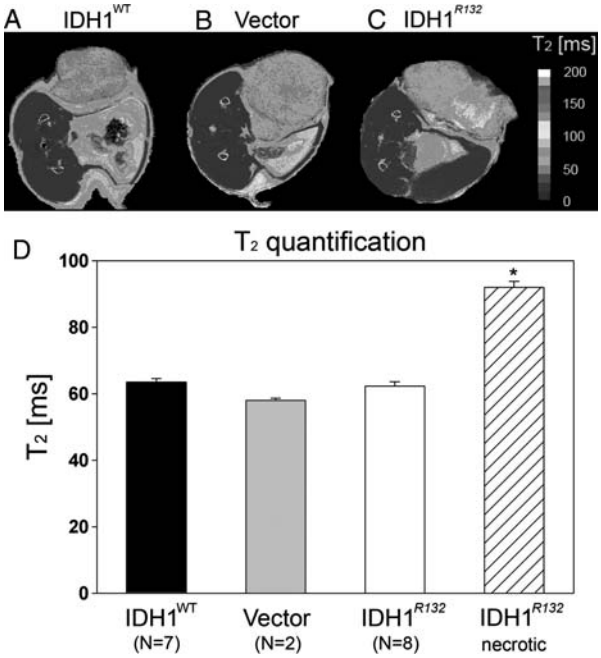

Fig. 3. (A–C) Representative T_2 maps showing T_2 distribution across different flank tumors. Color scale represents different T_2 values. (D) T_2 quantification for all 3 tumor types expressed as mean T_2 values ± SD. Notice similar T_2 distributions except for the necrotic area in IDH1^{R132} tumor (C) with elevated T_2 values, $^*P < .05$ ANOVA with Holm–Sidak correction for multiple pairwise comparison.

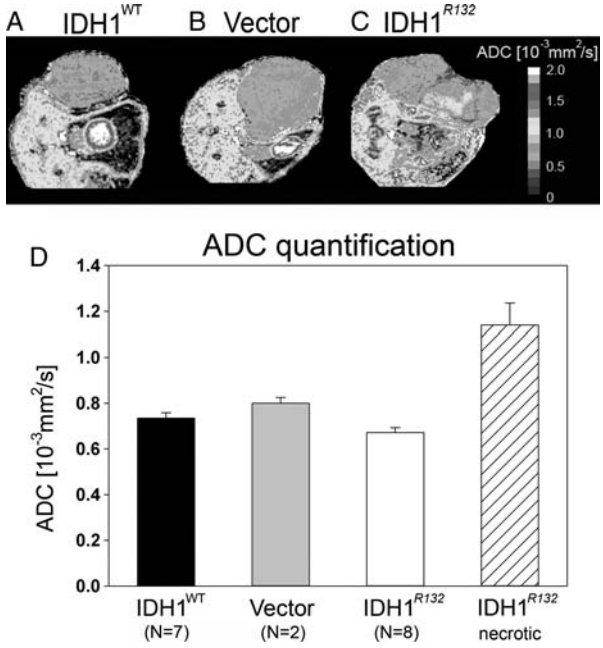

Fig. 4. (A–C) Representative ADC maps showing ADC distribution across different flank tumors. Color scale represents different ADC values. (D) ADC quantification for all 3 tumor types expressed as mean ADC values ± SD. Notice similar ADC distributions except for the necrotic area in IDH1^{R132} tumor (C) with elevated ADC values, $^*P < .05$ ANOVA with Holm–Sidak correction for multiple pairwise comparison.

($P < .05$, ANOVA with Holm–Sidak post hoc test) compared with IDH1^{R132} (Fig. 2D).

Quantification of T_2 and ADC

Increased T_2 values within tumor tissue are typically attributed to the presence of vasogenic edema or macroscopic necrosis. In the absence of vasogenic edema or necrosis, lower T_2 values are expected. No significant differences (1-way ANOVA) in T_2 values were detected between IDH1^{R132} (62.3 ± 3.5 ms), IDH1^{WT} (63.5 ± 2.8 ms), and U87-vector (57.9 ± 1.2 ms) flank tumors (Fig. 3D). However, flank tumors formed from IDH1^{R132}-overexpressing U87 cells had clear areas of macroscopic necrosis with significantly elevated T_2 values (ANOVA with Holm–Sidak post hoc test, $P < .05$) compared with T_2 values within the nonnecrotic region (91.9* ± 3.6 62 ms; Fig. 3D). Additionally, no significant differences in ADC (1-way ANOVA, $P > .05$), a surrogate for tumor cell density,[26,27] were found among flank tumors of nonnecrotic-region IDH1^{R132} ($0.672 \pm 0.052 \times 10^{-3}$ mm^2/s), IDH1^{WT} ($0.734 \pm 0.057 \times 10^{-3}$ mm^2/s), and U87-vector control ($0.800 \pm 0.057 \times 10^{-3}$ mm^2/s) (Fig. 4D); however, the necrotic region of the tumors overexpressing IDH1^{R132} had significantly higher ADC values ($1.140 \pm 0.192 \times 10^{-3}$ mm^2/s) compared with the nonnecrotic region of these tumors (ANOVA with Holm–Sidak post hoc test, $P < .05$), presumably owing to decreased cell density and increased extracellular space, as expected for necrotic areas.

MR Perfusion

Independent of IDH1^{R132} or IDH1^{WT} expression, all flank tumors had a similar pattern of contrast enhancement, with an enhancing periphery and non-enhancing T_1 hypointense central region (Fig. 5A–C). The slowest-growing WT tumors had a slightly larger area of contrast enhancement compared with IDH1^{R132} and U87-vector tumors. Central regions exhibiting MR signal intensity consistent with necrosis exhibited very low perfusion, whereas regions with contrast enhancement on postcontrast T_1-weighted images appeared to have elevated perfusion (Fig. 5D–F). Relative TBF was not significantly different among flank tumors of IDH1^{R132} (mean ± SEM = 25.01 ± 10.328 mL/100 mg tissue/min), IDH1^{WT} (22.29 ± 7.748 mL/100 mg tissue/min), and U87-vector (12.20 ± 1.69 mL/100 mg tissue/min) (1-way ANOVA on ranks; Fig. 5G), suggesting a similar degree of vascularity among these tumors.

H&E Histology and IDH1^{R132} Immunohistochemistry

IDH1^{R132} immunohistochemistry confirmed the presence of *IDH1*^{R132} in flank tumors overexpressing IDH1^{R132}, but not *IDH1*^{WT} and U87-vector (Fig. 6A–D). Interestingly, while most cells appeared immunoreactive

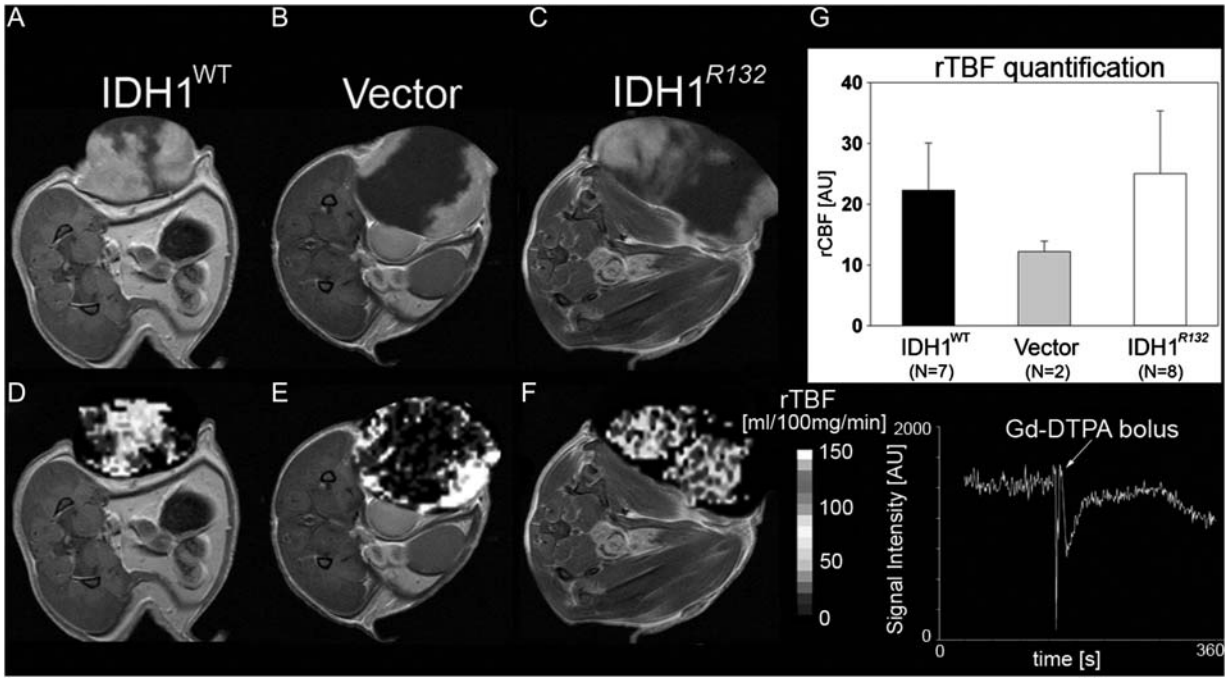

Fig. 5. (A–C) Representative postcontrast T_1-weighted MRIs of IDH1^{WT}, vector-control, and IDH1^{R132} flank tumors. Notice areas void of contrast agent enhancement in all 3 tumor types. (D–F) Representative perfusion images (color scale represents different perfusion values, mL/100 mg tissue/min) with DSC signal intensity bolus curve. Areas of reduced perfusion were present in all 3 tumor types, usually matched with areas of poor contrast enhancement. Some of the geometric distortion is due to use of echo planar imaging sequence for DSC perfusion. (G) Graph representing relative tumor blood flow (rTBF) measurements expressed as mean blood flow values ± SEM.

for IDH1^{R132}, there were occasional cells that did not stain (Fig. 6D). Whether these represented tumor cells that had lost *IDH1*^{R132} or connective cells from the vasculature or other sources is not clear (Fig. 6D). H&E histology confirmed a necrotic area of ~40%–50% (Fig. 6H) in flank tumors overexpressing IDH1^{R132} compared with a region of necrosis of ~10%–20% observed in IDH1^{WT} and vector-control tumors (Fig. 6E–H).

Discussion

The current study is the first controlled experiment validating the link between noninvasive 2-HG detection using MRS and the *IDH1*^{R132} mutation in glioma cells. IDH1^{R132} overexpression in U87 cells led to in vivo detectable levels of 2-HG using MRS, providing further evidence of a causal relationship between the IDH1 mutation and 2-HG production, as previously suggested by in vivo human glioma data.[15–18] We also found that glutamate was significantly altered in the IDH1 mutants, while other clinically relevant MRI parameters, including T_2 and ADC quantification, were not significantly different.

Previous investigations have demonstrated that MRS can be used to detect 2-HG in human glioma patients.[16–18,27] Similar to the findings from human data, we found that the IDH1 mutation resulted in a 2-HG resonance at ~2.25 ppm chemical shift, adjacent to the glutamate and glutamine peaks. As expected, cells overexpressing IDH1^{WT} lacked this metabolic peak. For our experiments, 2-HG levels were estimated to be between 10 mM and 20 mM in IDH1^{R132} flank tumors, somewhat higher than the 2–9 mM range reported for humans.[16] The glutamate resonance (at 2.31–2.35 ppm) was sufficiently distinct from the 2-HG resonance to prevent contamination of the 2-HG peak, which has been a limitation of 2-HG quantification in tumors with MRS performed on clinical (1.5T and 3T) scanners. Given the similarity of the IDH1 mutant spectra in the current study with those previously published from in vivo human data, this use of IDH1^{R132} mutant overexpressing cell lines has provided further evidence that the IDH1^{R132} mutation is responsible for the 2-HG peak and that this resonance is not related to tumor grade or other confounding factors.

Reduced glutamate levels have previously been reported for human oligodendroglioma-derived cell lines stably expressing the IDH1^{R132} mutation.[28] The IDH1^{R132} mutation also has been associated with decreased α-ketoglutarate (1 of the metabolic precursors for glutamate synthesis, and the substrate for production of 2-HG by IDH^{R132}).[12] Since α-ketoglutarate is integral to the Kreb's cycle, reduced glutamate could indicate compromised oxidative metabolism, increased utilization of glutamate for acetyl coenzyme A synthesis, or irreversible conversion to 2-HG. Glutamate is thought to mediate epileptic seizures induced by brain tumors,[29]

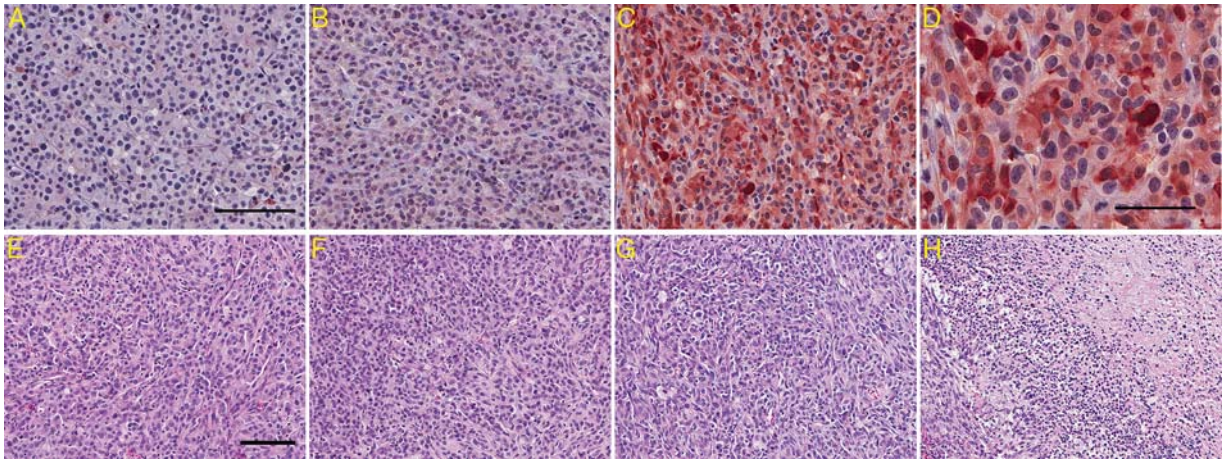

Fig. 6. IDH1 staining and H&E histology of tumors overexpressing IDH^{WT}, vector control, and IDH1^{R132}. (A–D) Representative IDH1 immunohistochemistry for (A) IDH1^{WT}, (B) vector control, and (C) IDH1^{R132} showing IDH1^{R132}-positive cells for only *IDH1*^{R132}-transduced gliomas; scale bar (A) represents 100 μm. (D) Higher magnification of IDH1^{R132} immunohistochemistry in IDH1^{R132} flank tumors shows that not all U87 cells are IDH1^{R132} positive; scale bar represents 50 μm. (E–G) Representative H&E staining for (E) IDH1^{WT}, (F) vector control, and (G) IDH1^{R132}; scale bar represents 100 μm. (H) H&E staining shows the necrotic region in the IDH1^{R132} flank tumor.

and therefore the relationship between the IDH1 mutation and glutamate levels could have important clinical implications, meriting further investigation.

Results from the current study suggest that IDH1^{R132} mutant tumors have larger areas of macroscopic necrosis defined by MR compared with IDH1^{WT}. Specifically, extensive areas of necrosis (~40%–50% of the entire tumor volume) were observed in all tumors overexpressing IDH1^{R132} ~21 days following injections, compared with <20% macroscopic necrosis observed in IDH1^{WT} or U87-vector flank tumors. It is conceivable that this may be due to slight size differences in the mutant tumors within the context of the current experiment, as more rapid tumor growth could occur quicker than the angiogenesis necessary to maintain a normoxic environment.[18,30,31] Alternatively, elevated levels of 2-HG could potentially be toxic to the tumor cells, leading to more extensive necrotic area. In humans, 2-HG toxicity is suggested by the observation that inborn errors of metabolism resulting in elevated 2-HG levels result in encephalopathy.[32,33] Direct toxicity of 2-HG to rat cerebral cortical slices has been demonstrated (at 5-mM concentration), in similar concentrations to those of 2-HG reported for gliomas,[11,14,31] and within the range of 2-HG levels calculated for the xenografts used in our study.[11,14,34] One caveat to this assumption, however, is that IDH1 mutant glioblastomas seem to have less necrosis than their WT counterparts, at least as detected by MRI.[35]

In summary, we have demonstrated that overexpression of the IDH1 mutation leads to detectable levels of 2-HG in a mouse glioma model that can be measured in vivo and noninvasively by MRS. This model system is of potential utility in establishing the relationships among 2-HG levels and treatment effect, outcomes, and other variables necessary to validate 2-HG as a clinically important biomarker for glioma.

Conflict of interest statement. None declared.

References

1. Parsons DW, Jones S, Zhang X, et al. An integrated genomic analysis of human glioblastoma multiforme. *Science*. 2008;321(5897):1807–1812.
2. Mardis ER, Ding L, Dooling DJ, et al. Recurring mutations found by sequencing an acute myeloid leukemia genome. *N Engl J Med*. 2009;361(11):1058–1066.
3. Green A, Beer P. Somatic mutations of IDH1 and IDH2 in the leukemic transformation of myeloproliferative neoplasms. *N Engl J Med*. 2010;362(4):369–370.
4. Ward PS, Patel J, Wise DR, et al. The common feature of leukemia-associated IDH1 and IDH2 mutations is a neomorphic enzyme activity converting alpha-ketoglutarate to 2-hydroxyglutarate. *Cancer Cell*. 2010;17(3):225–234.
5. Kang MR, Kim MS, Oh JE, et al. Mutational analysis of IDH1 codon 132 in glioblastomas and other common cancers. *Int J Cancer*. 2009;125(2):353–355.
6. Sjoblom T, Jones S, Wood LD, et al. The consensus coding sequences of human breast and colorectal cancers. *Science*. 2006;314(5797):268–274.
7. Lopez GY, Reitman ZJ, Solomon D, et al. IDH1(R132) mutation identified in one human melanoma metastasis, but not correlated with metastases to the brain. *Biochem Biophys Res Commun*. 2010;398(3):585–587.
8. Yan H, Parsons DW, Jin G, et al. IDH1 and IDH2 mutations in gliomas. *N Engl J Med*. 2009;360(8):765–773.

9. Xu X, Zhao J, Xu Z, et al. Structures of human cytosolic NADP-dependent isocitrate dehydrogenase reveal a novel self-regulatory mechanism of activity. *J Biol Chem*. 2004;279(32):33946–33957.
10. Nobusawa S, Watanabe T, Kleihues P, Ohgaki H. IDH1 mutations as molecular signature and predictive factor of secondary glioblastomas. *Clin Cancer Res*. 2009;15(19):6002–6007.
11. Dang L, White DW, Gross S, et al. Cancer-associated IDH1 mutations produce 2-hydroxyglutarate. *Nature*. 2009;462(7274):739–744.
12. Zhao S, Lin Y, Xu W, et al. Glioma-derived mutations in IDH1 dominantly inhibit IDH1 catalytic activity and induce HIF-1alpha. *Science*. 2009;324(5924):261–265.
13. Garber K. Oncometabolite? IDH1 discoveries raise possibility of new metabolism targets in brain cancers and leukemia. *J Natl Cancer Inst*. 2010;102(13):926–928.
14. Xu W, Yang H, Liu Y, et al. Oncometabolite 2-hydroxyglutarate is a competitive inhibitor of alpha-ketoglutarate-dependent dioxygenases. *Cancer Cell*. 2011;19(1):17–30.
15. Andronesi OC, Kim GS, Gerstner E, et al. Detection of 2-hydroxyglutarate in IDH-mutated glioma patients by in vivo spectral-editing and 2D correlation magnetic resonance spectroscopy. *Sci Transl Med*. 2012;4(116):116ra114.
16. Choi C, Ganji SK, Deberardinis RJ, et al. 2-hydroxyglutarate detection by magnetic resonance spectroscopy in IDH-mutated patients with gliomas. *Nat Med*. 2012;18:624–629.
17. Elkhaled A, Jalbert LE, Phillips JJ, et al. Magnetic resonance of 2-hydroxyglutarate in IDH1-mutated low-grade gliomas. *Sci Transl Med*. 2012;4(116):116ra115.
18. Pope WB, Prins RM, Albert Thomas M, et al. Non-invasive detection of 2-hydroxyglutarate and other metabolites in IDH1 mutant glioma patients using magnetic resonance spectroscopy. *J Neurooncol*. 2012;107(1):197–205.
19. Nikiforova MN, Hamilton RL. Molecular diagnostics of gliomas. *Arch Pathol Lab Med*. 2011;135(5):558–568.
20. Boxerman JL, Schmainda KM, Weisskoff RM. Relative cerebral blood volume maps corrected for contrast agent extravasation significantly correlate with glioma tumor grade, whereas uncorrected maps do not. *AJNR Am J Neuroradiol*. 2006;27(4):859–867.
21. Tkac I, Starcuk Z, Choi IY, Gruetter R. In vivo 1H NMR spectroscopy of rat brain at 1 ms echo time. *Magn Reson Med*. 1999;41(4):649–656.
22. Provencher SW. Estimation of metabolite concentrations from localized in vivo proton NMR spectra. *Magn Reson Med*. 1993;30(6):672–679.
23. Bal D, Gryff-Keller A. H-1 and C-13 NMR study of 2-hydroxyglutaric acid and its lactone. *Magnetic Resonance in Chemistry*. 2002;40(8):533–536.
24. Gregorian C, Nakashima J, Dry SM, et al. PTEN dosage is essential for neurofibroma development and malignant transformation. *Proc Natl Acad Sci U S A*. 2009;106(46):19479–19484.
25. Capper D, Zentgraf H, Balss J, Hartmann C, von Deimling A. Monoclonal antibody specific for IDH1 R132H mutation. *Acta Neuropathol*. 2009;118(5):599–601.
26. Gupta RK, Cloughesy TF, Sinha U, et al. Relationships between choline magnetic resonance spectroscopy, apparent diffusion coefficient and quantitative histopathology in human glioma. *J Neurooncol*. 2000;50(3):215–226.
27. Lazovic J, Jensen MC, Ferkassian E, Aguilar B, Raubitschek A, Jacobs RE. Imaging immune response in vivo: cytolytic action of genetically altered T cells directed to glioblastoma multiforme. *Clin Cancer Res*. 2008;14(12):3832–3839.
28. Reitman ZJ, Jin G, Karoly ED, et al. Profiling the effects of isocitrate dehydrogenase 1 and 2 mutations on the cellular metabolome. *Proc Natl Acad Sci U S A*. 2011;108(8):3270–3275.
29. Buckingham SC, Campbell SL, Haas BR, et al. Glutamate release by primary brain tumors induces epileptic activity. *Nat Med*. 2011;17(10):1269–1274.
30. Altman DA, Atkinson DS, Jr., Brat DJ. Best cases from the AFIP: glioblastoma multiforme. *Radiographics*. 2007;27(3):883–888.
31. Jain RK, di Tomaso E, Duda DG, Loeffler JS, Sorensen AG, Batchelor TT. Angiogenesis in brain tumours. *Nat Rev Neurosci*. 2007;8(8):610–622.
32. Struys EA. D-2-Hydroxyglutaric aciduria: unravelling the biochemical pathway and the genetic defect. *J Inherit Metab Dis*. 2006;29(1):21–29.
33. Kolker S, Mayatepek E, Hoffmann GF. White matter disease in cerebral organic acid disorders: clinical implications and suggested pathomechanisms. *Neuropediatrics*. 2002;33(5):225–231.
34. Latini A, da Silva CG, Ferreira GC, et al. Mitochondrial energy metabolism is markedly impaired by D-2-hydroxyglutaric acid in rat tissues. *Mol Genet Metab*. 2005;86(1–2):188–199.
35. Carrillo JA, Lai A, Nghiemphu PL, et al. Relationship between tumor enhancement, edema, IDH1 mutational status, MGMT promoter methylation, and survival in glioblastoma. *AJNR Am J Neuroradiol*. 2012;33:1349–1355.